Philosophical Magazine
Publication details, including instructions for authors and subscription information:
http://www.tandfonline.com/loi/tphm20

Phase field modelling of grain boundary motion driven by curvature and stored energy gradients. Part I: theory and numerical implementation

G. Abrivard [a], E.P. Busso [a], S. Forest [a] & B. Appolaire [b]

[a] Centre des Matériaux, Mines ParisTech/CNRS UMR 7633, BP 87, 91003 Evry cedex, France

[b] LEM, ONERA/CNRS UMR 104, 29 Av. Division Leclerc, BP 72, 92322 Châtillon, France

Version of record first published: 18 Sep 2012.

To cite this article: G. Abrivard, E.P. Busso, S. Forest & B. Appolaire (2012): Phase field modelling of grain boundary motion driven by curvature and stored energy gradients. Part I: theory and numerical implementation, Philosophical Magazine, 92:28-30, 3618-3642

To link to this article: http://dx.doi.org/10.1080/14786435.2012.713135

Philosophical Magazine
Vol. 92, Nos. 28–30, 1–21 October 2012, 3618–3642

Taylor & Francis
Taylor & Francis Group

Phase field modelling of grain boundary motion driven by curvature and stored energy gradients. Part I: theory and numerical implementation

G. Abrivard[a], E.P. Busso[a]*, S. Forest[a] and B. Appolaire[b]

[a]*Centre des Matériaux, Mines ParisTech/CNRS UMR 7633, BP 87, 91003 Evry cedex, France;* [b]*LEM, ONERA/CNRS UMR 104, 29 Av. Division Leclerc, BP 72, 92322 Châtillon, France*

(*Received 2 December 2011; final version received 5 July 2012*)

During thermo-mechanical processing, the strain energy stored in the microstucture of an FCC polycrystalline aggregate is generally reduced by physical phenomena controlled, at least partially, by mechanisms involving dislocation cell or grain boundary motion such as recovery, recrystallisation and grain growth. This work presents a novel coupled phase field-single crystal constitutive framework capable of describing the microstructural evolution driven by grain boundary curvature and/or stored energy during recrystallisation and grain growth. Thus, the minimisation of stored and grain boundary energies provides the driving force for grain boundary motion. To describe interface motion, a phase field model taking into account the stored energy distribution is formulated and implemented within a continuum mechanics framework. The single crystal constitutive behaviour is described using a dislocation mechanics-based crystallographic formulation. The coupling between the grain boundary kinematics and the crystal plasticity formulation is made through the dislocation densities and the grain orientations. Furthermore, the free energy parameters are calibrated from existing Read–Shockley boundary energy data and those describing grain boundary mobilities from published experimental data.

Keywords: phase field; grain boundary; recrystallisation; stored energy; crystal plasticity; finite elements

1. Introduction

In high temperature metal forming processes, metallic alloys undergo important microstructural changes due to the combined effects of thermo-mechanical loads which strongly affect their mechanical properties. The evolution of the microstructure under such conditions generally involves strain hardening, dynamic recovery, recrystallisation and grain growth. In mechanisms such as recrystallisation and grain growth, grain boundary motion is driven by the need to minimise its grain boundary and stored strain energies. The understanding and prediction of such phenomena is

*Corresponding author. Email: esteban.busso@ensmp.fr

ISSN 1478–6435 print/ISSN 1478–6443 online

http://dx.doi.org/10.1080/14786435.2012.713135
http://www.tandfonline.com

crucial for an accurate control of the mechanical properties of metal forming components and for their optimisation.

Generally, the prediction of physical phenomena associated with a moving interface is of interest in a wide range of areas, such as phase transformations (e.g. [1–6]), or recrystallisation (e.g. [7–9]). In the past, several modelling approaches have been used to study grain boundary motion: Monte Carlo [10–12], cellular automata [13–15], vertex techniques [16,17], level set [18], finite element [19] and phase field methods [9,20–22]. Amongst all the above numerical approaches, the phase field method exhibits a major advantage: it does not explicitly need to track the moving grain boundary or interface. Instead, sharp grain boundaries or interfaces are replaced by interfacial regions of finite width, defined through the evolution of suitable fields (the so-called phase fields), which evolve continuously but sharply across the interface. Two main types of phase field models are used to study polycrystalline materials: (i) those which rely on a different phase field variable to describe each individual grain, and (ii) those where a single field is required to represent the orientation distribution of all grains. The first category has been relied upon to study mainly grain growth in [21,22] and, more recently, recrystallisation [8,9]. The second category has two attractive features, both conceptual and practical: (i) it satisfies the property requirement that the free energy should be independent of grain orientation, and (ii) only one field is necessary to describe an infinite number of orientations. This latter approach was originally proposed by Kobayashi, Warren and Craig Carter (henceforth referred to as KWC) to describe the impingement and growth of grains following solidification [23,24]. In the same spirit, it is worth mentioning the work of Lusk [25], which relies on the microforces framework (e.g. [26]) to be followed in the present paper.

In addition to a suitable approach to model grain boundary motion, the description of the initial microstructural state which drives recrystallisation processes is also essential for a proper prediction of the coupled deformation-kinetics phenomena. For instance, the microstructural conditions which prevail before the onset of recrystallisation have been based on, e.g. measured microstructural characteristics [27], numerical predictions obtained from crystal plasticity [9], and internal state variable visco-plastic constitutive approaches relating the onset to a critical mean dislocation spacing [7].

In this work, a novel coupled phase field–crystal plasticity framework is proposed to describe the kinetics of moving grain boundaries and interfaces when driven by curvature and local stored energy gradients associated with inelastic deformation. The phase field model of KWC, which accounts only for the interface curvature as a driving force for grain boundary motion, is here extended in a thermodynamically consistent way to incorporate explicitly stored energy gradients as an additional driving force. First, it benefits from the conceptual and practical advantages of the single phase field mentioned above as opposed to those relying on multi-phase fields, e.g. [8,9]. Second, the coupling with the stored strain energy is straightforward and does not require any averaging procedure as in [28]. The framework relies on two phase field variables to represent the characteristics of the mobile grain boundaries, namely the crystallinity and the grain orientation, as well as on suitable balance laws and constitutive equations. The crystallographic deformation is described by the dislocation mechanics based single crystal model proposed by Cheong et al. [29],

which enables the contributions of dislocations of pure type to the overall deformation behaviour to be distinguished. The coupling between the phase field and the crystal plasticity formulation is done via (i) the incorporation of the stored strain energy calculated at the crystal plasticity level within the free energy functional of the phase field model, and (ii) a static recovery term in the evolutionary equations of the individual dislocation densities to account for the annihilation of dislocations by a passing grain boundary. Finally, the resulting coupled constitutive framework is implemented numerically into the finite element method and then calibrated from analytical solutions and available data.

The paper is structured as follows. The phase field formulation is first presented in Section 2, where details are given of the proposed free energy functional, the constitutive equation derived from the first and second laws of thermodynamics, and the resulting evolution equations for the phase field variables. This section finishes with the numerical implementation of the phase field formulation in the finite element method. Section 3 introduces the single crystal formulation used in this work, and Section 4 deals with the calibration of both the phase field parameters and the crystal plasticity formulation. Here, the grain boundary energy given by the phase field model is calibrated against the Read–Shockley energy, and the grain boundary mobilities and the crystal plasticity model parameters against published data. In a companion paper [30], the coupled stress-phase field framework will be validated by comparing the model predictions to analytical solutions and experimental data. The main aspects of the grain boundary motion predictions will be discussed, and finite element simulations of static recrystallisation phenomena in a polycrystal aggregate will be presented and analysed.

2. Phase field formulation

2.1. *Free energy*

The formulation to be presented next is two dimensional, which considerably simplifies the description of a grain boundary. A grain boundary separates two crystallographic regions with different orientations. Grain boundary regions lack the order of crystals and are composed of lattice defects extending over thicknesses of the order of a few atomic layers (Figure 1a). A two-dimensional (2D) description of a grain boundary requires only two geometrical degrees of freedom: the inclination angle of the boundary plane between the two neighbouring crystals, and the crystallographic misorientation, $\Delta\theta$ (see Figure 1a). In this work, the free energy will be assumed to be independent of the inclination angle, and to be an isotropic function of misorientation.

The general form of the free energy function developed here was inspired by that previously proposed by KWC [24]. In the KWC formulation, the evolution of the crystalline grains is described in terms of two fields: the orientation, θ, with respect to some reference frame, and the crystallinity, η, which describes the local crystalline order. Crystals are assumed to have N-fold symmetry, thus all values of θ lie in a reduced domain $[-\pi/N;\ \pi/N]$. Furthermore, an upper bound value of $\eta = 1$ is arbitrarily assigned to a perfect crystal, and a lower bound value of $\eta = 0$ to complete disorder (Figure 1b, c). The stored energy is included into the free energy functional

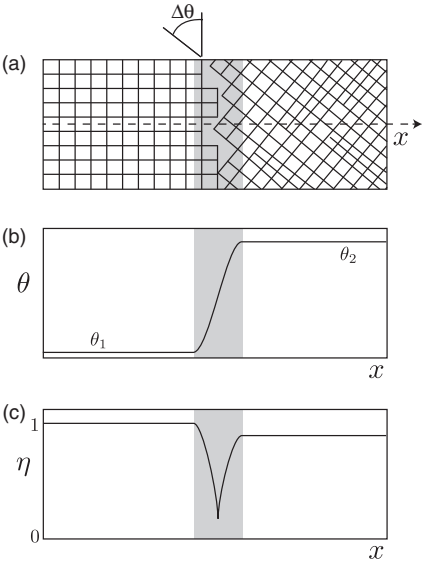

Figure 1. (a) Schematics of a bicrystal composed of a perfect (left-hand side) and a dislocation-containing (right-hand side) crystal, and typical profiles across the grain boundary (along x) of (b) orientation angle, θ, and (c) crystallinity, η.

as follows. Before deformation, all grains are assumed to have a perfect crystal lattice, thus the crystal order, η, is constant and equal to 1 inside the grains. Within the grain boundary, the crystallinity varies between 0 and 1 as a function of the misorientation between grains. In the present extension of the KWC model, we introduce the fact that, during deformation, the dislocation density increases inside the grains thus introducing a certain loss of crystallinity and leading to $\eta < 1$. Nevertheless, note that the transgranular lattice disorder induced by the heterogeneity of the deformation remains considerably smaller than that within the high-angle grain boundaries (see Figure 1c). A measure of the lattice disorder induced by the deformation in a crystal can be the stored energy due to statistically stored dislocations. This energy is greater in high angle grain boundaries than within the grains due to their greater disorder. In this work, the energy stored during the deformation, E_{st}, is introduced explicitly in a rotation-invariant free energy functional as follows,

$$\begin{aligned}\mathcal{F}(\eta,\theta,E_{\mathrm{st}}) &= \int_{\mathcal{V}} \psi(\eta,\nabla\eta,\nabla\theta,E_{\mathrm{st}})\mathrm{d}\mathcal{V} \\ &= \int_{\mathcal{V}} \left(f(\eta) + C\,\bar{E}_{\mathrm{st}}\,\eta + \frac{\alpha^2}{2}|\nabla\eta|^2 + g(\eta)|\nabla\theta| + h(\eta)|\nabla\theta|^2 \right)\mathrm{d}\mathcal{V}, \end{aligned} \tag{1}$$

where $f(\eta)$ is a homogeneous free energy density function accounting for the penalty due to grain boundary disorder. Following the work of [24], this function is chosen so as to yield a single well with a minimum at $\eta = 1$ for perfect crystals,

$$f(\eta) = \frac{\omega^2}{2}(1-\eta)^2. \tag{2}$$

Here, ω is a positive constant related to the grain boundary energy (Section 4.1.1). The second term in Equation (1) is chosen to be proportional to the normalised stored energy density, $\bar{E}_{\mathrm{st}}$, and scaled by a positive constant, C. This term is linear in η since the stored energy due to the presence of dislocations is more likely to affect a perfect crystal and is of no consequence to regions with a complete disordered state. The stored energy density in Equation (1), E_{st}, is normalised by the maximum value of the grain boundary energy, E_{hgb}, to prevent any disordered lattice state from becoming more stable than that in the grain boundaries. Thus, E_{hgb} is taken to be the energy of high angle grain boundaries (neglecting any Σ type boundaries), so that $\bar{E}_{\mathrm{st}} = E_{\mathrm{st}}/E_{\mathrm{hgb}}$. The third term in Equation (1) introduces a penalty for the gradients in the order parameter η, with α a positive constant which is also related to the grain boundary energy (Section 4.1.1). Finally, the linear term, $|\nabla\theta|$, is required to obtain a localised and stable grain boundary while the term $h(\eta)|\nabla\theta|^2$ is necessary for a grain boundary to migrate [31]. Note also that $h(\eta)$ and $g(\eta)$ are monotonically increasing functions of η, as will be shown in Section 4.1.1.

2.2. *Principle of virtual power*

A continuum-mechanics framework to describe dynamic problems has been proposed in [4,26,32] based on a balance law for generalised forces associated with the equilibrium of atoms and defect configurations. In the case of recrystallisation, the short-range transport of atoms between adjacent mismatched lattices is introduced via dissipative generalised forces that perform work over the motion of grain boundaries at continuum length-scales. In this section, the same approach is used to determine the balance and constitutive laws associated with the free energy. The microstructure is represented by the two fields previously defined, namely the crystallinity, η, and the crystal orientation, θ. The generalised forces associated with both fields are characterised by microstresses and by microforces. Here, $\underline{\xi}_\eta$ is the work conjugate microstress to $\nabla\eta$, and π_η and π_η^{ext} are, respectively, the work conjugate internal and external microforces to η. Furthermore, $\underline{\xi}_\theta$ is the microstress associated with $\nabla\theta$, and π_θ and $\pi_\theta^{\mathrm{ext}}$ are, respectively, the internal and external microforces associated with θ. The method of virtual powers due to the work performed by these forces is used to determine the balance law equations. The virtual power of internal forces is expressed as:

$$\mathcal{P}^{(i)} = \int_{\mathcal{D}} \left(\pi_\eta \dot{\eta} - \underline{\xi}_\eta \cdot \nabla\dot{\eta} + \pi_\theta \dot{\theta} - \underline{\xi}_\theta \cdot \nabla\dot{\theta} \right) \mathrm{d}\mathcal{V}, \tag{3}$$

$$= \int_{\mathcal{D}} \left(\left(\nabla \cdot \underline{\xi}_\eta + \pi_\eta \right)\dot{\eta} + \left(\nabla \cdot \underline{\xi}_\theta + \pi_\theta \right)\dot{\theta} \right) \mathrm{d}\mathcal{V} - \int_{\partial\mathcal{D}} \left(\left(\underline{\xi}_\eta \cdot \underline{n} \right)\dot{\eta} + \left(\underline{\xi}_\theta \cdot \underline{n} \right)\dot{\theta} \right) \mathrm{d}\mathcal{S} \tag{4}$$

and that due to the external forces, including distance and contact forces, as

$$\mathcal{P}^{(e)} = \int_{\mathcal{D}} \left(\pi_\eta^{\mathrm{ext}}\, \dot{\eta} + \pi_\theta^{\mathrm{ext}}\, \dot{\theta} \right) \mathrm{d}\mathcal{V}, \tag{5}$$

$$\mathcal{P}^{(c)} = \int_{\partial\mathcal{D}} \left(\pi_\eta^c \,\dot{\eta} + \pi_\theta^c \,\dot{\theta}\right) \mathrm{d}\mathcal{S}. \tag{6}$$

If the power of inertial microforces are neglected, then the principle of virtual power states that,

$$\mathcal{P}^{(i)} + \mathcal{P}^{(e)} + \mathcal{P}^{(c)} = 0, \qquad \forall \mathcal{D} \in \mathcal{V},\ \forall (\dot{\eta}, \dot{\theta}). \tag{7}$$

Substitution of Equations (4)–(6) into Equation (7) yields,

$$\int_{\mathcal{D}} \left(\left(\nabla \cdot \underline{\xi}_\eta + \pi_\eta + \pi_\eta^{\mathrm{ext}}\right)\dot{\eta} + \left(\nabla \cdot \underline{\xi}_\theta + \pi_\theta + \pi_\theta^{\mathrm{ext}}\right)\dot{\theta} \right) \mathrm{d}\mathcal{V} = 0, \quad \forall \mathcal{D} \in \mathcal{V},\ \forall (\dot{\eta}, \dot{\theta}). \tag{8}$$

Assuming that the field variables θ and η are continuous on $\mathcal{V}$, then the following local equilibrium equations are found,

$$\nabla \cdot \underline{\xi}_\theta + \pi_\theta + \pi_\theta^{\mathrm{ext}} = 0 \quad \text{in } \mathcal{V}, \tag{9}$$

$$\nabla \cdot \underline{\xi}_\eta + \pi_\eta + \pi_\eta^{\mathrm{ext}} = 0 \quad \text{in } \mathcal{V}. \tag{10}$$

When external forces are neglected, the principle of virtual power becomes,

$$\int_{\partial\mathcal{D}} \left(\left(\underline{\xi}_\eta \cdot \underline{n} - \pi_\eta^c\right)\dot{\eta} + \left(\underline{\xi}_\theta \cdot \underline{n} - \pi_\theta^c\right)\dot{\theta} \right) \mathrm{d}\mathcal{S}, \quad \forall \mathcal{D} \in V,\ \forall (\dot{\eta}, \dot{\theta}), \tag{11}$$

from which the following boundary conditions are obtained,

$$\underline{\xi}_\eta \cdot \underline{n} = \pi_\eta^c \quad \text{on } \partial\mathcal{V}, \tag{12}$$

$$\underline{\xi}_\theta \cdot \underline{n} = \pi_\theta^c \quad \text{on } \partial\mathcal{V}. \tag{13}$$

2.3. *Constitutive phase field equations*

Neglecting any acceleration power, the energy conservation is written as:

$$\dot{E} = \mathcal{P}^{(e)} + \mathcal{P}^{(c)} + Q, \tag{14}$$

or equivalently,

$$\dot{E} = -\mathcal{P}^{(i)} + Q. \tag{15}$$

Let e_{int} be the internal energy per unit volume, and $\underline{q}$ the heat flux density vector. Then the energy balance reads

$$\dot{e}_{\mathrm{int}} = \underline{\xi}_\eta \cdot \nabla\dot{\eta} + \underline{\xi}_\eta \cdot \nabla\dot{\theta} - \pi_\eta \dot{\eta} - \pi_\theta \,\dot{\theta} - \nabla \cdot \underline{q}. \tag{16}$$

According to the thermodynamics of irreversible processes, the entropy principle is given as

$$\dot{s} + \nabla \cdot \left(\frac{\underline{q}}{T}\right) \geq 0, \tag{17}$$

where T denotes the absolute temperature and s the entropy per unit volume.

By recalling that the free energy density is $\psi = e_{\text{int}} - Ts$, and combining the energy and entropy equations, the Clausius–Duhem inequality is obtained. Then,

$$-(s\,\dot{T} + \dot{\psi}) + \underline{\xi}_{\eta} \cdot \nabla\dot{\eta} + \underline{\xi}_{\eta} \cdot \nabla\dot{\theta} - \pi_{\eta}\,\dot{\eta} - \pi_{\theta}\,\dot{\theta} - \frac{1}{T}\,\underline{q} \cdot \nabla T \geq 0. \tag{18}$$

For simplicity, the formulation will henceforth be expressed for isothermal conditions, thus any temperature rate dependence term will be omitted. The free energy density is only dependent on η, $\nabla\eta$, and $\nabla\theta$. Therefore,

$$\dot{\psi}(\eta, \nabla\eta, \nabla\theta) = \frac{\partial\psi}{\partial\eta}\,\dot{\eta} + \frac{\partial\psi}{\partial\nabla\eta} \cdot \nabla\dot{\eta} + \frac{\partial\psi}{\partial\nabla\theta} \cdot \nabla\dot{\theta}, \tag{19}$$

and Equation (18) becomes,

$$\begin{aligned}\left(-\frac{\partial\psi}{\partial\eta} - \pi_{\eta}\right)\dot{\eta} - \pi_{\theta}\,\dot{\theta} + \left(-\frac{\partial\psi}{\partial\nabla\eta} + \underline{\xi}_{\eta}\right) \cdot \nabla\dot{\eta} \\ + \left(-\frac{\partial\psi}{\partial\nabla\theta} + \underline{\xi}_{\theta}\right) \cdot \nabla\dot{\theta} - \frac{1}{T}\,\underline{q} \cdot \nabla T \geq 0.\end{aligned} \tag{20}$$

The microstresses $\underline{\xi}_{\eta}$ and $\underline{\xi}_{\theta}$ are assumed to be independent of $\dot{\eta}$ and $\dot{\theta}$. They satisfy the following equations of state,

$$\underline{\xi}_{\eta} = \frac{\partial\psi}{\partial\nabla\eta}, \tag{21}$$

$$\underline{\xi}_{\theta} = \frac{\partial\psi}{\partial\nabla\theta}, \tag{22}$$

$$s = -\frac{\partial\psi}{\partial T}. \tag{23}$$

Then,

$$-\left(\frac{\partial\psi}{\partial\eta} + \pi_{\eta}\right)\dot{\eta} - \pi_{\theta}\,\dot{\theta} \geq 0, \tag{24}$$

$$\pi_{\eta} = -\frac{\partial\psi}{\partial\eta} + \pi_{\eta}^{\text{non}}, \tag{25}$$

$$\pi_{\theta} = \pi_{\theta}^{\text{non}}. \tag{26}$$

The functions π_{η}^{non} and $\pi_{\theta}^{\text{non}}$ represent non-equilibrium contributions to the internal forces, π_{η} and π_{θ}, respectively. To be consistent with the second law of thermodynamics, π_{η}^{non} and $\pi_{\theta}^{\text{non}}$ should satisfy the following condition obtained by substituting Equations (25) and (26) into (24),

$$\pi_{\eta}^{\text{non}}\,\dot{\eta} + \pi_{\theta}^{\text{non}}\,\dot{\theta} \leq 0. \tag{27}$$

2.4. *Evolution equations of the field variables η and θ*

From the free energy functional, Equation (1), the following constitutive relations can be derived:

$$\underline{\xi}_{\eta} = \frac{\partial \psi}{\partial \nabla \eta} = \alpha^2 \, \nabla \eta, \tag{28}$$

$$\underline{\xi}_{\theta} = \frac{\partial \psi}{\partial \nabla \theta} = g(\eta) \frac{\nabla \theta}{|\nabla \theta|} + 2\, h(\eta) \nabla \theta, \tag{29}$$

$$\pi_{\eta} = -\frac{\partial \psi}{\partial \eta} + \pi_{\eta}^{\text{non}} = -f'(\eta) - C\bar{E}_{\text{st}} - g'(\eta)|\nabla \theta| - h'(\eta)|\nabla \theta|^2 + \pi_{\eta}^{\text{non}}, \tag{30}$$

$$\pi_{\theta} = \pi_{\theta}^{\text{non}}, \tag{31}$$

with

$$\pi_{\eta}^{\text{non}} = -\tau_{\eta} \, \dot{\eta}, \tag{32}$$

$$\pi_{\theta}^{\text{non}} = -\tau_{\theta} \, \dot{\theta}. \tag{33}$$

Here, τ_{η} and τ_{θ} are inverse mobilities, always posivite, related to the grain boundary mobility in a non-trivial manner [31]. They are expressed as follows:

$$\tau_{\eta} = \beta_{\eta}(T) \, \omega^2, \tag{34}$$

$$\tau_{\theta} = \beta_{\theta}(T) \, \omega^2 \, P_m(\eta) \, P_r(\eta, \nabla \eta), \tag{35}$$

where β_{η} and β_{θ} are temperature-dependent parameters which define the time-scales for the evolutions of crystallinity and orientation, respectively. Both of them are assigned the same temperature dependence through an inverse Arrhenius law involving an activation energy, Q, so as to recover the usual temperature dependence of grain boundary mobilities:

$$\beta_{\eta}(T) = \beta_{\eta}^{0} \, \exp\left(\frac{Q}{kT}\right), \tag{36}$$

$$\beta_{\theta}(T) = \beta_{\theta}^{0} \, \exp\left(\frac{Q}{kT}\right). \tag{37}$$

It is worth noting that Equation (33) introduces the possibility of lattice rotation, at a rate controlled by the functions $P_m(\eta)$ and $P_r(\eta, \nabla \eta)$. Following KWC, $P_m(\eta) = \eta^2$ since the rotation of a disordered state has no physical meaning. Moreover, as shown in [31], an additional function P_r must be introduced in order to prevent the rotation rate from diverging for the sharp interface limit. For that purpose, we have chosen the following expression:

$$P_r(\eta, \nabla \eta) = 1 + \beta_r \left[1 - \exp(-\beta_s \eta / |\nabla \eta|)\right] \tag{38}$$

where β_r is a constant such that $\beta_r \gg 1$ so that the characteristic times for the spurious rotation of the grain core region are very large. In contrast, the parameter β_s defines a length-scale, typically of the order of the grain boundary width. It must be stressed that Equation (38) is different from the expression proposed by KWC [24]. Indeed, due to stable states with $\eta < 1$ when $\bar{E}_{\mathrm{st}} > 0$, it was found more suitable to rely on $\eta/|\nabla\eta|$ rather than on $|\nabla\theta|$ to define the maximum allowed rotations. Finally, it should be noted that by choosing $\tau_\eta^0 \ll \tau_\theta^0$ (or equivalently $\beta_\eta \ll \beta_\theta$), grain rotations in the absence of mechanical stresses can be inhibited.

Substituting the expressions for the microstresses and microforces (Equations 28–31) in the associated balance law equations (9)–(10), the following evolutionary equations for η and θ are obtained,

$$\tau_\eta \dot{\eta} = \alpha^2 \nabla^2 \eta - f'(\eta) - C\bar{E}_{\mathrm{st}} - g'(\eta)|\nabla\theta| - h'(\eta)|\nabla\theta|^2, \tag{39}$$

$$\tau_\theta \dot{\theta} = \nabla \cdot \left(2\, h(\eta)\nabla\theta + g(\eta)\frac{\nabla\theta}{|\nabla\theta|} \right). \tag{40}$$

It is worth stressing that the presence of $\bar{E}_{\mathrm{st}}$ in Equation (39) introduces a constraint on the model parameters. Within the core of a grain, $\nabla\eta \approx 0$ and $\nabla\theta = 0$, thus Equation (39) yields a particular value of crystallinity in stationary conditions, $\bar{\eta}$. Here,

$$0 = -f'(\bar{\eta}) - C\bar{E}_{\mathrm{st}} = \omega^2(1 - \bar{\eta}) - C\bar{E}_{\mathrm{st}}. \tag{41}$$

From Equation (41), one obtains the intra-granular value of crystallinity,

$$\bar{\eta} = 1 - \bar{E}_{\mathrm{st}}\, C/\omega^2. \tag{42}$$

Since $0 \leq \bar{\eta} \leq 1$, then it can be seen from Equation (42) that the following condition must be satisfied by the model parameters,

$$\bar{E}_{\mathrm{st}}\, C/\omega^2 < 1. \tag{43}$$

2.5. *Evolution equation of the stored energy*

In physical phenomena involving moving grain boundaries, the migration through a given region of the crystal lattice restores a dislocation-free lattice and decreases the stored energy. Experimental evidence is shown in the TEM micrograph of Figure 2a, where a dislocation-free region appeared to have been left in the wake of a moving grain boundary. Such a situation is depicted by the stationary profile of η across a grain boundary of width 2δ at $x/\delta = \epsilon \approx 0$ illustrated in Figure 2b. This profile was obtained for a heterogeneous distribution of the stored energy: $\bar{E}_{\mathrm{st}} = 0$ and $\eta = \bar{\eta} = 1$ for $x/\delta < (\epsilon - 1)$; and $\bar{E}_{\mathrm{st}} \approx 0.65$ and $\eta = \bar{\eta} \approx 0.35$ for $x/\delta > \epsilon + 1$ (considering $C/\omega^2 = 1$).

To account for the changes due to grain boundary migration, the evolution of the stored energy has to be coupled to the evolutions of η and θ. In the region in front of the grain boundary where $\dot{\eta} < 0$ (dark grey in Figure 2b), the dislocation density and

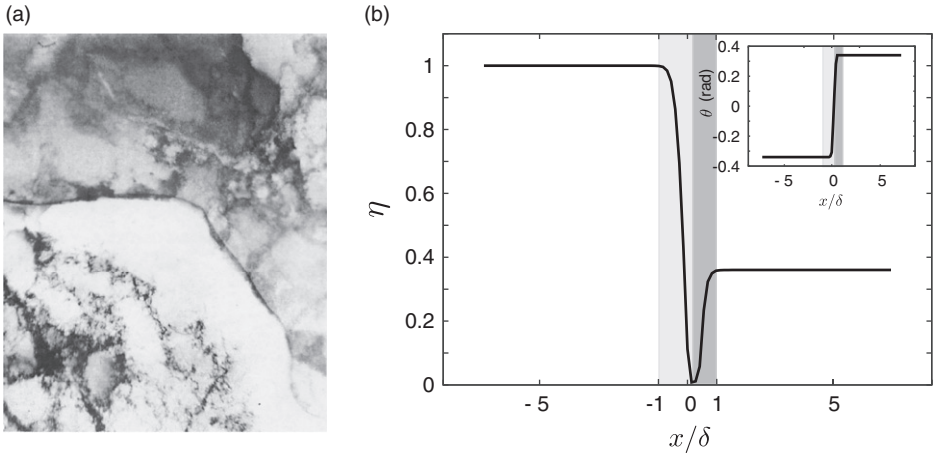

Figure 2. (a) TEM observation of the migration of a grain boundary leaving a dislocation free region in its wake [33]. (b) Stationary profile of crystallinity η with a heterogeneous distribution of stored energy E_{st} (corresponding orientation profile is shown in the inset).

E_{st} remain unchanged. In contrast, they decrease behind the grain boundary, *viz*. in the region where $\dot{\eta} > 0$ (light grey region in Figure 2b). This can be expressed in a simple form as,

$$\dot{E}_{\mathrm{st}} = \begin{cases} -E_{\mathrm{st}}\, C_d\, A(|\nabla\theta|)\, \dot{\eta}, & \text{if } \dot{\eta} > 0, \\ 0, & \text{if } \dot{\eta} \leq 0, \end{cases} \tag{44}$$

where C_d is a positive constant. The aim of the function A ($|\nabla\theta|$) is to localise the annihilation of the stored energy at the very centre of the grain boundaries. Here, the following function is used,

$$A(|\nabla\theta|) = \tanh\left(|\nabla\theta|^2\right). \tag{45}$$

Considering the scales over which θ varies within a grain boundary, then $A(|\nabla\theta|) \approx 1$ as soon as $|\nabla\theta| \neq 0$. To illustrate typical evolutions of the stored energy within the core of a grain boundary (dark grey region in Figure 2), consider simply that $A(|\nabla\theta|) = 1$. In that case, integration of Equation (44) for $\dot{\eta} > 0$ gives,

$$E_{\mathrm{st}} = B \exp(-C_d\, \eta) \tag{46}$$

where B is a constant determined from the initial conditions. Consider then that initially at time $t = 0$ s, $E_{\mathrm{st}} = E_{\mathrm{st0}}$, and $\eta_0 = 1 - \bar{E}_{\mathrm{st0}}\, C/\omega^2$ from Equation (42) (where $\bar{E}_{\mathrm{st0}} = E_{\mathrm{st0}}/E_{\mathrm{hgb}}$), which constitutes an upper bound value for η. Then Equation (46) becomes,

$$E_{\mathrm{st}} = E_{\mathrm{st0}} \exp\left(C_d (1 - \bar{E}_{\mathrm{st0}}\, C/\omega^2 - \eta)\right). \tag{47}$$

Figure 3 shows how the stored energy, normalised by E_{hgb}, varies with η according to Equation (47), assuming $\bar{E}_{\mathrm{st0}} = 0.6$ and $C/\omega^2 = 1$. The stored energy decreases as η tends to 1, and this happens more rapidly with increasing values of the parameter C_d.

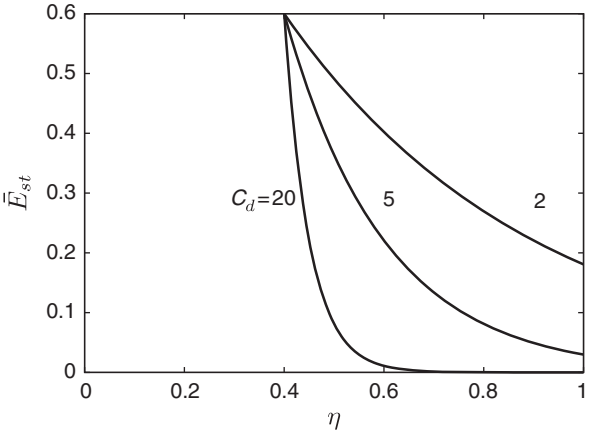

Figure 3. Evolution of the stored energy given by (47), normalised by E_{hgb}, from an initial value of $\bar{E}_{\mathrm{st0}} = 0.6$ as a function of η for different values of C_d (assuming $C/\omega^2 = 1$).

When C_d is sufficiently large, $\bar{E}_{\mathrm{st}}$ goes to zero for values of $\eta < 1$ located inside the grain boundary, which implies a complete statically recovered (dislocation free) state.

2.6. *Implementation of the phase-field formulation in the finite element method*

The numerical implementation of the phase field model into the finite element method is an adaptation of the algorithm proposed in [1] for a phase transformation problem.

2.6.1. *Variational formulation*

The variational formulation of the phase field partial differential equations directly follows from the principle of virtual power outlined in Section 2.2. From Equations (3)–(7), one finds

$$\mathcal{F}(\eta^*, \mathcal{V}) = \int_{\mathcal{V}} \left(\pi_\eta \eta^* - \underline{\xi}_\eta \cdot \nabla \eta^*\right) \mathrm{d}\mathcal{V} + \int_{\partial\mathcal{V}} \pi_\eta^c \, \eta^* \, \mathrm{d}\mathcal{S} = 0, \tag{48}$$

$$\mathcal{F}(\theta^*, \mathcal{V}) = \int_{\mathcal{V}} \left(\pi_\theta \theta^* - \underline{\xi}_\theta \cdot \nabla \theta^*\right) \mathrm{d}\mathcal{V} + \int_{\partial\mathcal{V}} \pi_\theta^c \, \theta^* \, \mathrm{d}\mathcal{S} = 0, \tag{49}$$

where η^* and θ^* are the virtual phase field variables.

The phase field problem is subject to the following initial conditions at time $t = 0$,

$$\eta(\underline{x}, t = 0) = \eta_0(\underline{x}), \tag{50}$$

$$\theta(\underline{x}, t = 0) = \theta_0(\underline{x}). \tag{51}$$

2.6.2. *Finite element discretisation*

The spatial discretisation is generalised to N elements, and the nodal degrees of freedom are taken to be the lattice order and the crystal orientation. The fields η and θ are approximated at position $\underline{x}$ within each element and at every time, t, in terms of their nodal values (with subscript i) and the interpolation functions, $N_i^e(\underline{x})$. Then,

$$\eta(\underline{x},t)=\sum_{i=1}^{n}N_i^e(\underline{x})\,\eta_i(t),\quad \theta(\underline{x},t)=\sum_{i=1}^{n}N_i^e(\underline{x})\,\theta_i(t), \tag{52}$$

$$\eta^*(\underline{x},t)=\sum_{i=1}^{n}N_i^e(\underline{x})\,\eta_i^*(t),\quad \theta^*(\underline{x},t)=\sum_{i=1}^{n}N_i^e(\underline{x})\,\theta_i^*(t), \tag{53}$$

$$\nabla\eta(\underline{x},t)=\sum_{i=1}^{n}B_i^e(\underline{x})\,\eta_i(t),\quad \nabla\theta(\underline{x},t)=\sum_{i=1}^{n}B_i^e(\underline{x})\,\theta_i(t), \tag{54}$$

where n is the number of nodes in the element, e, containing $\underline{x}$. The matrix B_i^e is defined by the first derivative of the shape functions, which in the 2D case, is

$$[B^e]=\begin{bmatrix}\dfrac{\partial N_1^e}{\partial x} & \dfrac{\partial N_2^e}{\partial x} & \cdots & \dfrac{\partial N_n^e}{\partial x}\\ \dfrac{\partial N_1^e}{\partial y} & \dfrac{\partial N_2^e}{\partial y} & \cdots & \dfrac{\partial N_n^e}{\partial y}\end{bmatrix}.$$

An implicit Euler scheme is implemented for the time discretisation [34]. Let $\eta(t)$ and $\theta(t)$ be the known values of these variables at time t, and $\eta(t+\Delta t)$ and $\theta(t+\Delta t)$ at time $t+\Delta t$. Thus, the latter can be expressed in terms of the time increment, Δt, as,

$$\eta(t=0)=\eta_0, \tag{55}$$

$$\theta(t=0)=\theta_0, \tag{56}$$

$$\eta(t+\Delta t)=\eta(t)+\dot{\eta}(t+\Delta t)\,\Delta t, \tag{57}$$

$$\theta(t+\Delta t)=\theta(t)+\dot{\theta}(t+\Delta t)\,\Delta t. \tag{58}$$

Here, η_0, θ_0 are the initial conditions for the lattice order and the crystal orientation. The residual of a generic finite element with volume $\mathcal{V}^e$ and surface $\partial\mathcal{V}^e$ can be found by substituting the expressions for the nodal degrees of freedom, Equations (52)–(53), into the conditions of the variational problem at each instant, $t>0$. Then,

$$\left\{R^e(\eta,\theta)\right\}=\begin{Bmatrix}R_\eta^e(\eta,\theta)\\ R_\theta^e(\eta,\theta)\end{Bmatrix},$$

where,

$$(R_\eta^e)_i=\int_{\mathcal{V}^e}N_i^e(\underline{x})\,\pi_\eta\,\mathrm{d}\mathcal{V}-\int_{\mathcal{V}^e}\left[B^e(\underline{x})\right]_{ij}\xi_{\eta j}\,\mathrm{d}\mathcal{V}+\int_{\partial\mathcal{V}^e}N_i^e(\underline{x})\,\pi_\eta^c\,\mathrm{d}\mathcal{S}=0, \tag{59}$$

$$(R^e_\theta)_i = \int_{\mathcal{V}^e} N^e_i(\underline{x})\,\pi_\theta\,\mathrm{d}\mathcal{V} - \int_{\mathcal{V}^e} \left[B^e(\underline{x})\right]_{ij}\xi_{\theta j}\,\mathrm{d}\mathcal{V} + \int_{\partial\mathcal{V}^e} N^e_i(\underline{x})\,\pi^c_\theta\,\mathrm{d}\mathcal{S} = 0, \tag{60}$$

are the element residuals for the variational formulation of the lattice order and crystal orientation, respectively. Note that equating the above residuals to zero follows from the requirement that Equations (48) and (49) should hold for arbitrary variations of η and θ.

The global residual vector is obtained by assembling the element residuals for all elements using the assembly matrix, $[A^e]$:

$$\left\{R(\eta,\theta)\right\} = \sum_{e=1}^{N}\left[A^e\right]\cdot\left\{R^e(\eta,\theta)\right\} = \left\{0\right\}. \tag{61}$$

Given a known set of values for the nodal degrees of freedom at time, t, and recalling that the residual vector is required to vanish at the end of the time step, $t+\Delta t$, then this leads to a resulting set of nonlinear equations expressed in terms of the unknown values of the nodal degrees of freedom at $(t+\Delta t)$. These equations are solved iteratively using a Newton–Raphson type method. The algorithm requires the calculation of the generalised stiffness matrix, which is obtained by derivation of the residual vectors (59) and (60) with respect to the independent degrees of freedoms, (η,θ):

$$\left[K^e_t\right] = \begin{bmatrix}[K^e_{\eta\eta}] & [K^e_{\eta\theta}]\\ [K^e_{\theta\eta}] & [K^e_{\theta\theta}]\end{bmatrix}.$$

Finally, the components of the element's generalised stifness matrix are given by,

$$(K^e_{\eta\eta})_{ij} = -\frac{\partial(R^e_1)_i}{\partial\eta^e_j} = \int_{\mathcal{V}^e} N^e_i\left(\partial\pi_\eta/\partial\eta^e_j\right)\mathrm{d}\mathcal{V} - \int_{\mathcal{V}^e}\left[B^e(\underline{x})\right]_{ik}\left[\partial\xi_{\eta_k}/\partial\eta^e_j\right]\mathrm{d}\mathcal{V}, \tag{62}$$

$$(K^e_{\eta\theta})_{ij} = -\frac{\partial(R^e_1)_i}{\partial\theta^e_j} = \int_{\mathcal{V}^e} N^e_i\left(\partial\pi_\eta/\partial\theta^e_j\right)\mathrm{d}\mathcal{V} - \int_{\mathcal{V}^e}\left[B^e(\underline{x})\right]_{ik}\left[\partial\xi_{\eta_k}/\partial\theta^e_j\right]\mathrm{d}\mathcal{V}, \tag{63}$$

$$(K^e_{\theta\eta})_{ij} = -\frac{\partial(R^e_2)_i}{\partial\eta^e_j} = \int_{\mathcal{V}^e} N^e_i\left(\partial\pi_\theta/\partial\eta^e_j\right)\mathrm{d}\mathcal{V} - \int_{\mathcal{V}^e}\left[B^e(\underline{x})\right]_{ik}\left[\partial\xi_{\theta_k}/\partial\eta^e_j\right]\mathrm{d}\mathcal{V}, \tag{64}$$

$$(K^e_{\theta\theta})_{ij} = -\frac{\partial(R^e_2)_i}{\partial\theta^e_j} = \int_{\mathcal{V}^e} N^e_i\left(\partial\pi_\theta/\partial\theta^e_j\right)\mathrm{d}\mathcal{V} - \int_{\mathcal{V}^e}\left[B^e(\underline{x})\right]_{ik}\left[\partial\xi_{\theta_k}/\partial\theta^e_j\right]\mathrm{d}\mathcal{V}. \tag{65}$$

3. Single crystal plasticity formulation coupled to the phase field variables

The dislocation mechanics based single crystal model used in this work is that proposed by Cheong et al. [29]. This model has been successfully applied to a series of mechanistic investigations of single crystal and polycrystalline alloys (e.g. see [35–37]. In this formulation, dislocations are discretised into edge and screw

components having intrinsically different relative mobilities and are subject to different dynamic recovery processes. The individual contributions of each dislocation type to the overall deformation behaviour can therefore be distinguished. Furthermore, the discretisations of the dislocations into pure edge and screw components enable their different energies per unit length to be taken into account in the formulation of the strain energy. A brief description of the single crystal model is presented next (refer to Cheong et al. [29] for further details).

3.1. *Thermodynamics single crystal framework*

The kinematics for single crystal deformation relies on the classical multiplicative decomposition of the deformation gradient, $\underset{\sim}{\boldsymbol{F}}$, into an elastic, $\underset{\sim}{\boldsymbol{F}}^{e}$, and a plastic, $\underset{\sim}{\boldsymbol{F}}^{p}$, component. The velocity gradient is defined as,

$$\underset{\sim}{\boldsymbol{L}}^{p} = \dot{\underset{\sim}{\boldsymbol{F}}}^{p} \cdot \underset{\sim}{\boldsymbol{F}}^{p-1} = \sum_{\alpha=1}^{N} \dot{\gamma}^{\alpha} m^{\alpha} \otimes n^{\alpha}, \tag{66}$$

where $\dot{\gamma}^{\alpha}$ represents the crystallographic slip rate on a generic slip system (α) defined by the dyadic product between its slip direction ($\mathbf{m}^{\alpha}$) and associated slip plane normal ($\mathbf{n}^{\alpha}$).

The slip rate, $\dot{\gamma}^{\alpha}$, is assumed to be dominated by the thermally activated glide of dislocations over forest obstacles and the proposed form of $\dot{\gamma}^{\alpha}$ is related to the resolved shear stress, τ^{α}, as

$$\dot{\gamma}^{\alpha} = \dot{\gamma}_0 \exp\left[-\frac{F_0}{kT} \left\{ 1 - \left\langle \frac{|\tau^{\alpha}| - S_T^{\alpha} \mu/\mu_0}{\hat{\tau}_0 \mu/\mu_0} \right\rangle^{p} \right\}^{q} \right] \mathrm{sgn}(\tau^{\alpha}), \tag{67}$$

which takes into account the temperature and stress dependence of the activation energy. In Equation (67), F_0 represents the Helmholtz free energy of activation – the total energy required for a dislocation to overcome an obstacle encountered during glide, k is the Boltzmann constant, $\dot{\gamma}_0$ is a reference slip rate and $\hat{\tau}_0$ is the maximum glide resistance at which dislocations can be mobilised without thermal activation. The exponents p and q describe the shape of the energy barrier versus the resolved shear stress profile. All elastic interactions are reduced to 0 K by the shear moduli ratio of μ/μ_0 at the temperatures T and 0 K, respectively. The athermal slip resistance, S_T^{α}, is defined as,

$$S_T^{\alpha} = \lambda \mu b^{\alpha} \sqrt{\textstyle\sum_{\beta=1}^{N} h^{\alpha\beta} \rho_T^{\beta}}\,, \tag{68}$$

where the overall dislocation density, ρ_T^{β}, is expressed in terms of the pure edge and pure densities, $\rho_{\perp}^{\beta}$ and $\rho_{\odot}^{\beta}$, respectively. Then,

$$\rho_T^{\beta} = \rho_{\perp}^{\beta} + \rho_{\odot}^{\beta}. \tag{69}$$

In Equation (68), λ is a statistical constant, b^{α} the Burgers vector, and $h^{\alpha\beta}$ represents the dislocation interaction matrix defined as,

$$h^{\alpha\beta} = \omega_1 + (1 - \omega_2)\, \delta^{\alpha\beta}, \tag{70}$$

where ω_1 and ω_2 are two cross-hardening constants and $\delta^{\alpha\beta}$ is the Kronecker delta.

In this work, an explicit link between the evolution of the microstructure, given by that of the dislocation population, and those of the phase field variables is established through a thermodynamically consistent framework. The slip system internal variable, S_T^α, can be expressed in terms of its corresponding thermodynamical state variable, denoted s^α. Furthermore, the inelastic part of the free energy function is given in terms of a generic function of s^α, namely ψ_s^α, as,

$$\psi = \sum_\alpha \psi_s^\alpha, \tag{71}$$

where the sum over (α) extends over all potentially active slip systems.

The relation between S_T^α and s^α can be found from Equation (71), since, by definition,

$$S_T^\alpha = \frac{\partial \psi}{\partial s^\alpha} = \frac{\partial \psi_s^\alpha}{\partial s^\alpha}. \tag{72}$$

The inelastic part of the free energy function can be expressed as,

$$\psi_s^\alpha = \frac{1}{2}\,\lambda\,\mu\,(s^\alpha)^2. \tag{73}$$

Then,

$$S_T^\alpha = \lambda \mu s^\alpha. \tag{74}$$

The stored energy for an associated crystallographic model, E_{st}, is given by the difference between the plastic work and the internal dissipation due to the dominant hardening mechanisms. It can be shown that [38],

$$E_{\mathrm{st}} = \int_0^t \left(\frac{\partial \psi}{\partial s^\alpha}\,\frac{\mathrm{d}s^\alpha}{\mathrm{d}t}\right)\mathrm{d}t = \int_0^t \sum_\alpha (S_T^\alpha\,\dot{s}^\alpha)\mathrm{d}t. \tag{75}$$

Note that the stored energy, E_{st}, from the previous equation is the same as the second energy term introduced in Equation (1) when $C = E_{\mathrm{hgb}}$ and $\eta = 1$. Thus, in this case, the standard crystal plasticity energy is recovered.

Use of Equations (68), (69) and (74) with the time derivative of Equation (75) yields an expression for the evolution of the stored energy in terms of those of the individual dislocation densities. Here,

$$\dot{E}_{\mathrm{st}} = \frac{1}{2}\,\lambda\,\mu\,b^2 \sum_{\alpha=1}^{N}\sum_{\beta=1}^{N} h^{\alpha\beta}(\dot{\rho}_\perp^\alpha + \dot{\rho}_\odot^\alpha), \tag{76}$$

where it is assumed that $b^\alpha = b$ for $\alpha = 1, \ldots, N$.

The evolution equations for the dislocation densities account for the competing dislocation storage-dynamic recovery processes prevalent in FCC metals and for the annihilation of dislocations in the wake of a moving grain boundary. They are expressed as,

$$\dot{\rho}_\perp^\alpha = \frac{C_\perp}{b}\left[K_\perp \sqrt{\textstyle\sum_{\beta=1}^{N} \rho_T^\beta} - 2d_\perp \rho_\perp^\alpha\right]|\dot{\gamma}^\alpha| - E_{\mathrm{st}} C_{\mathrm{st}}\, A(|\nabla\theta|)\dot{\eta}, \tag{77}$$

$$\dot{\rho}^{\alpha}_{\odot} = \frac{C_{\odot}}{b}\left[K_{\odot}\sqrt{\sum_{\beta=1}^{N}\rho^{\beta}_{T}} - \rho^{\alpha}_{\odot}\left\{K_{\odot}\pi {d_{\odot}}^{2}\sqrt{\sum_{\beta=1}^{N}\rho^{\beta}_{T}} + 2\,d_{\odot}\right\}\right]|\dot{\gamma}^{\alpha}| - E_{\mathrm{st}}\,C_{\mathrm{st}}\,A(|\nabla\theta|)\,\dot{\eta}. \tag{78}$$

The last term in the above equations introduces an explicit coupling with the phase field variables (η, θ) to account for the static recovery type-mechanism discussed earlier in the text and described by Equation (44). Furthermore, the parameters $\{C_{\perp}, C_{\odot}\}$ describe the relative contributions to the overall slip from edge and screw dislocations, while $\{K_{\perp}, K_{\odot}\}$ are mobility constants associated with their respective mean free paths. Finally, recovery processes are associated with the parameters $\{d_{\perp}, d_{\odot}\}$, which represent critical annihilation distances between opposite sign dislocations for both edge and screw types. Substitution of the evolution equations (77) and (78) into (76) results in a general expression for the evolution of the stored energy. In order to formulate the expressions for $\dot{\mathrm{E}}_{\mathrm{st}}$ consistently in both the phase field and the crystal plasticity models, consider Equation (76) with (77) and (78) in the absence of slip (viz., when $|\dot{\gamma}^{\alpha}| = 0$). Then,

$$\dot{E}_{\mathrm{st}} = -\lambda\,\mu\,b^{2}\sum_{\alpha=1}^{N}\sum_{\beta=1}^{N}h^{\alpha\beta}\,E_{\mathrm{st}}\,C_{\mathrm{st}}\,A(|\nabla\theta|)\,\dot{\eta}. \tag{79}$$

Equating Equations (44) and (79) and recalling Equation (70) leads to the following expression for the parameter, C_d, in Equation (44):

$$C_d \;=\; C_{\mathrm{st}}\lambda\mu b^{2}N\,(1 + N\,\omega_1 - \omega_2), \tag{80}$$

in terms of the single crystal constants $\lambda, \mu, b, N, \omega_1$ and ω_2.

The theory is completed by considering the elastic constitutive law,

$$\underset{\sim}{\boldsymbol{T}} = \underset{\approx}{\boldsymbol{C}} : \underset{\sim}{\boldsymbol{E}}^{e}. \tag{81}$$

Here, $\underset{\sim}{\boldsymbol{T}}$ is the lattice-based second Piola–Kirchhoff stress tensor, $\underset{\approx}{\boldsymbol{C}}$ is the anisotropic elasticity tensor, while $\underset{\sim}{\boldsymbol{E}}^{e}$ $(= [\underset{\sim}{\boldsymbol{F}}^{eT}\cdot\underset{\sim}{\boldsymbol{F}}^{e} - \underset{\sim}{\boldsymbol{I}}]/2)$ is the Green–Lagrange strain tensor, with $\underset{\sim}{\boldsymbol{I}}$, the second-order identity tensor. Furthermore, $\underset{\sim}{\boldsymbol{T}}$ can be expressed as,

$$\underset{\sim}{\boldsymbol{T}} = (\det\underset{\sim}{\boldsymbol{F}}^{e})\underset{\sim}{\boldsymbol{F}}^{e-1}\cdot\underset{\sim}{\boldsymbol{\sigma}}\cdot\underset{\sim}{\boldsymbol{F}}^{e-T}, \tag{82}$$

in terms of the Cauchy stress tensor, $\underset{\sim}{\boldsymbol{\sigma}}$.

3.2. *Finite element implementation*

Details of the numerical implementation of the above constitutive theory in the finite element method using finite strain assumptions are given separately, see [29] and [39]. The coupling between the phase field and the crystal plasticity formulation within the finite element framework is outlined in Figure 4, which presents a flow chart illustrating the exchange of information between the phase field and the crystal plasticity levels. Each of the two problems is solved independently and sequentially and the data is exchanged at the end of each time increment. Nevertheless, note that even though the phase field variables are incorporated in the solution of the

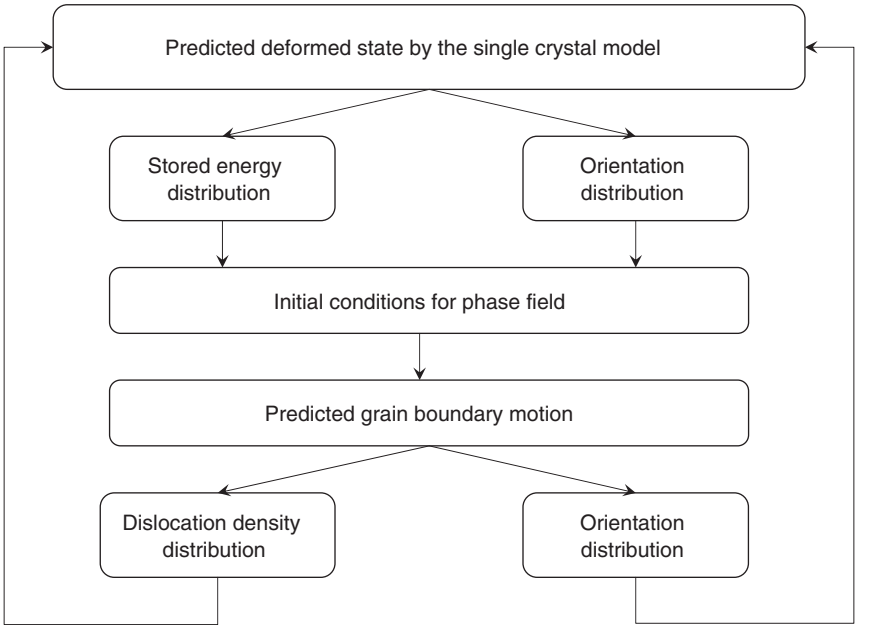

Figure 4. Flow chart illustrating the coupling between dislocation density evolution with the static recovery associated with grain boundary motion.

mechanical problem via Equations (77) and (78), the mechanical analysis is not fully coupled with the phase field since the stresses are not accounted for in the description of grain boundary migration. The loss of accuracy associated with such one-way coupling would depend on the relative effect of the stress on the kinetics of grain boundary migration. However, this type of experimental information is not generally readily available. It should also be pointed out that both the phase field and the single crystal domains rely on the same finite element spatial discretisation, so as to minimise related errors. Further details about the numerical implementation of the coupled problem are given in [39].

4. Calibration of the models

The coupled phase field–crystal plasticity framework will be calibrated for pure aluminium.

4.1. *Phase field parameters*

4.1.1. *Grain boundary energy*

For the purpose of calibrating the phase field parameters related to the grain boundary free energy, it is first convenient to classify grain boundaries into (i) those whose misorientation angle, $\Delta\theta$ ($=|\theta_2 - \theta_1|$ in Figure 1), is greater than a certain transitional value, denoted $\Delta\theta_{\text{tran}}$, generally known as high angle grain boundaries;

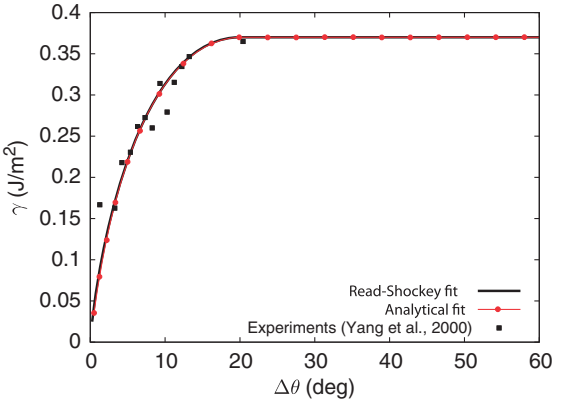

Figure 5. Grain boundary energy versus misorientation obtained experimentally by Yang et al. [41], and analytically using the Read–Shokley model (Equation 83), and the phase field model with $g(\eta)$ given by Equation (90).

and (ii) those whose misorientation is less than $\Delta\theta_{\text{tran}}$, referred to as low angle grain boundaries. The transition angle is typically taken to be around 15° for materials with cubic crystal lattices. In this work, it will be assumed to be ~19° to achieve an optimal fit to available experimental data (see below). For misorientation angles smaller than $\Delta\theta_{\text{tran}}$, the grain boundary energy exhibits a logarithmic dependency on misorientation and can be well described by the Read–Shockley model [40], as shown in Figure 5. Note that this model was originally developed for a symmetric tilt boundary. For greater misorientations (neglecting special Σ grain boundaries), the grain boundary energy can be assumed to remain constant and equal to γ_{hgb}, that is, independent of misorientation and boundary plane. Thus,

$$\gamma = \begin{cases} \gamma_{\text{hgb}}\, \Delta\bar{\theta}\left(1 - \ln \Delta\bar{\theta}\right) & \text{for } \Delta\theta \le \Delta\theta_{\text{tran}}, \\ \gamma_{\text{hgb}} & \text{for } \Delta\theta > \Delta\theta_{\text{tran}}, \end{cases} \tag{83}$$

where $\Delta\bar{\theta}$ is the misorientation angle normalised by $\Delta\theta_{\text{tran}}$. It is important to note that the stored energy density, E_{st}, is expressed in J m^{-3} while the grain boundary energy is associated with a surface and, therefore, expressed in J m^{-2}. However, the thickness of a typical grain boundary, δ, is approximately made up of three to four atomic layers, as illustrated in Figure 1a. Consider then that if $\delta \approx 3.5a_p$, where a_p is the thickness of an atomic layer as given by the size of the crystal's primitive unit cell, then for FCC crystals

$$\delta \approx 3.5a_p = \frac{14}{\sqrt{2}} R_{\text{at}}, \tag{84}$$

where R_{at} is the atomic radius. For pure Al, $R_{\text{at}} = 125\,\text{pm}$ and the high angle grain boundary energy is $\gamma_{\text{hgb}} = 0.37\,\text{J m}^{-2}$, as obtained from the work of [41] on aluminium foils. Therefore the energy density of a high angle grain boundary of thickness δ is,

$$E_{\text{hgb}} \approx \frac{\gamma_{\text{hgb}}}{\delta} \approx 300 \times 10^6\,\text{J m}^{-3}. \tag{85}$$

To recover the grain boundary energies predicted by Equation (83), we have followed the KWC approach [24,31] and considered a static planar grain boundary separating two semi-infinite perfect crystals ($\bar{E}_{st}=0$) with a given misorientation, $\Delta\theta$. The grain boundary energy is defined as the excess free energy per unit area and can therefore be obtained by integrating Equation (1) over the whole system, i.e. along the x-axis normal to the grain boundary plan. For a static grain boundary, $h(\eta)|\nabla\theta|^2$ can be omitted as it introduces only a minor contribution. In that case, the integration of Equation (40) to determine θ gives a step function with a jump of magnitude equal to the misorientation angle, $\Delta\theta$, at the grain boundary position ($x=0$). Likewise, the integration of Equation (39) to determine η results in a function which exhibits a cusp at $x=0$ and a minimum value, η_c, which satisfies the implicit relation $g'(\eta_c)\Delta\theta = 2\alpha\sqrt{2f(\eta_c)}$. Using these solutions, Equation (1) can be split into two contributions (refer to [23,24,31] for full details):

$$\gamma = \int_{-\infty}^{+\infty} \psi \, \mathrm{d}x = \gamma_{\mathrm{dis}} + \gamma_{\mathrm{or}}, \tag{86}$$

where γ_{dis} arises from the disorder within the grain boundary,

$$\gamma_{\mathrm{dis}} = \int_{-\infty}^{\infty} \left(f(\eta) + \frac{\alpha^2}{2} \left| \frac{\mathrm{d}\eta}{\mathrm{d}x} \right|^2 \right) \mathrm{d}x = 2\alpha \int_{\eta_c}^{1} \sqrt{2f(\eta)} \mathrm{d}\eta, \tag{87}$$

and γ_{or} accounts for the misorientation between the two abutting grains,

$$\gamma_{\mathrm{or}} = \int_{-\infty}^{\infty} g(\eta) \left| \frac{\mathrm{d}\theta}{\mathrm{d}x} \right| \mathrm{d}x = g(\eta_c)\, \Delta\theta, \tag{88}$$

For the specific form of the free energy density function, $f(\eta)$, given by Equation (2), Equation (86) yields the following excess free energy associated with the grain boundary,

$$\gamma = \alpha\omega(1-\eta_c)^2 + g(\eta_c)\, \Delta\theta, \tag{89}$$

where α and ω are constants. A third-order polynomial was chosen for $g(\eta)$:

$$g(\eta) = a_1\eta + a_2\eta^2 + a_3\eta^3, \tag{90}$$

where a_1, a_2 and a_3 are parameters which, together with Equation (89)'s α and ω, need to be fitted to the experimental data of [41], and hence match Equation (83)'s predictions (see Figure 5). Solving the resulting implicit relation for η_c from the previous equations, one obtains

$$\eta_c = \frac{1}{3a_3\chi} \left(-(a_2\chi + 1) + \sqrt{(a_2\chi+1)^2 - 3a_3\chi(a_1\chi - 2)} \right), \tag{91}$$

with $\chi = \Delta\theta/(\alpha\omega)$. Substitution of (91) into Equation (89) provides an analytical expression for the grain boundary energy as predicted by the KWC model. Good agreement is obtained between this expression and Equation (83) using the set of parameters given in Table 1 for the static case. It can be seen in Figure 5 that the Read–Shockley model and the analytical solution for misorientations smaller than

Table 1. Phase field parameters.

	α ($\sqrt{\text{J m}^{-1}}$)	ω ($\sqrt{\text{J m}^{-3}}$)	a_1 (J m^{-2})	a_2 (J m^{-2})	a_3 (J m^{-2})	d (J m^{-1})
Static	0.04	7.50	2.1	0.95	1.35	–
Dynamic	0.04	7.50	1.0	0.95	1.35	0.45

the transitional angle are indistinguishable. Recall that the Read–Schockley model is only valid for misorientations up to this transitional angle.

In dynamic situations, it is necessary to include $h(\eta)|\nabla\theta|^2$ in the free energy functional, as mentioned previously. The following form has been chosen for $h(\eta)$:

$$h(\eta) = d\,\eta^2 + e, \tag{92}$$

where we have added a positive constant e to the quadratic part originally proposed by KWC to provide an indirect measure of the length over which $\nabla\theta$ extends. When e increases, the thickness of the grain boundary, its ability to move [30], and its energy increase. A parametric study has been performed to estimate the values of e which can be used in dynamic calculations without changing dramatically the grain boundary properties. The parameters used are given in Table 1 and the results shown in Figure 6. First, the same good agreement with Equation (83) has been achieved using $e = 0$ and the same parameters as for the static case, except for $a_1 = 1\,\text{J m}^{-2}$ due to the presence of $h(\eta)|\nabla\theta|^2$ with $d = 0.45\,\text{J m}^{-1}$ (see Table 1). For $e \leq 10^{-3}\,\text{J m}^{-3}$, changes in the overall behaviour of γ versus $\Delta\theta$ are negligible. For greater values, typically of the order of $10^{-2}\,\text{J m}^{-3}$, a significant increase in γ is observed for large misorientations, that is when $\Delta\theta > 20^\circ$. It is worth noting that grain boundaries with small misorientation angles still follow a Read–Shockley type behaviour.

4.1.2. *Grain boundary mobility*

The mechanism of boundary migration depends on several factors, which include the grain boundary structure, the temperature and the nature and magnitude of the forces acting on it. The migration rate is usually reported to be proportional to the total driving force, P, acting upon the grain boundary:

$$v = MP, \tag{93}$$

where M is the so-called grain boundary mobility. As shown in [31] with an asymptotic analysis of the model, when P involves only the energy, γ, and the curvature, κ, of the grain boundary ($P = \kappa\gamma$), M is a complex function of the phase field parameters involving non-trivial integrals, $\mathcal{I}$ and $\mathcal{J}$, which need to be computed numerically. For the general case:

$$1/M \propto \beta_\eta \mathcal{I} + \beta_\theta \mathcal{J}. \tag{94}$$

The dependence of M on temperature, generally observed to follow an Arrhenius law, $M = M_0 \exp(-Q/(RT))$, can be reproduced by calibrating the activation energy in Equations (36) and (37) based on available experimental data. It is important to

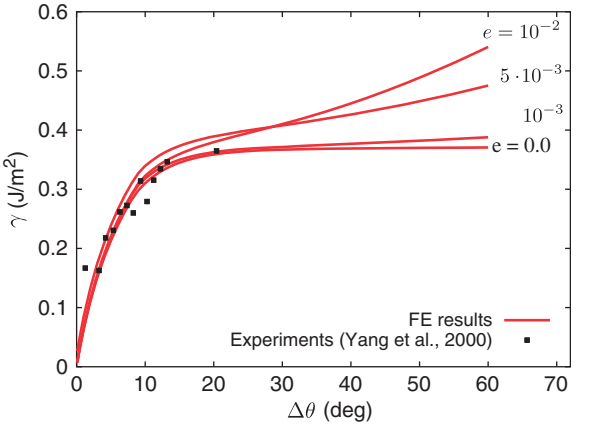

Figure 6. Grain boundary energies versus misorientation predictions obtained using increasing values of the parameter e in Equation (92).

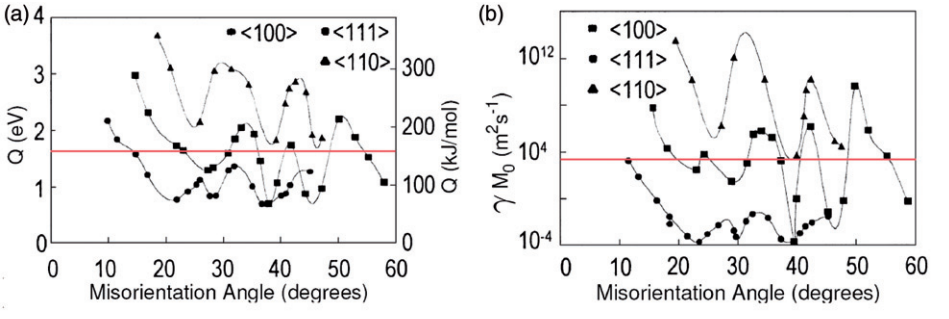

Figure 7. Grain boundary mobility (a) activation energy (Q) and (b) pre-exponential factor (M_0) as a function of misorientation angle: experiments from [42] (symbols) and average values chosen in the present work (red horizontal lines).

point out that, even though the activation energy Q and the pre-exponential factors β_η^0 and β_θ^0 in Equations (36) and (37) are assumed to be constant, measurements on specially misoriented boundaries (i.e. low-Σ boundaries) have shown that Q and ($M_0\gamma$) exhibit cusps at certain misorientations. This can be observed in the experimental measurements of [42], reported in Figure 7. Here, average values of those quantities (given by the (red) horizontal lines in Figure 7) are chosen, namely $M_0\gamma = 4 \times 10^3\,\mathrm{m^2\,s^{-1}}$ and $Q = 1.7\,\mathrm{eV}$. Finally, individual values of β_η^0 and β_θ^0 will be determined based on the average values of $M_0\gamma$ obtained from full analyses of grain boundary mobilities. This is to be given in the companion article [30] for the case of the shrinkage of a circular grain embedded in a largely misoriented matrix.

4.2. *Single crystal model parameters*

The parameters of the single crystal model used here are those published in the literature for aluminium. The anisotropic elasticity parameters, C_{11}, C_{12} and C_{44}, are

Table 2. Flow rule parameters for Al.

$\widehat{\tau}_0$ (MPa)	p	q	$\dot{\gamma}_0$ (s^{-1})	F_0 (J)
8.0	0.141	1.1	1.73×10^6	3.00×10^{-19}

Table 3. Additional single crystal model parameters for Al.

	C_i	K_i/b^α (mm^{-1})	d_i (nm)	Y_i^α (μm)
Edge	0.5	55×10^3	7.0	162
Screw	0.5	110×10^3	35.0	81
$\mu = 45.0$ GPa	$\lambda = 0.3$	$b^\alpha = 0.286$ nm	$\omega_1 = 1.5$	$\omega_2 = 1.2$

temperature-dependent and each have been approximated by a polynomial relation (units in GPA) [43]:

$$C_{11} = 123.32 + (6.70 \times 10^{-8})\, T^3 - (1.13 \times 10^{-4})\, T^2 - (7.88 \times 10^{-3})\, T, \tag{95}$$

$$C_{12} = 70.65 + (4.41 \times 10^{-8})\, T^3 - (7.55 \times 10^{-5})\, T^2 - (4.00 \times 10^{-3})\, T, \tag{96}$$

$$C_{44} = 31.21 + (7.05 \times 10^{-9})\, T^3 - (1.22 \times 10^{-5})\, T^2 - (8.33 \times 10^{-3})\, T. \tag{97}$$

The flow rule defined by Equation (67) contains five material parameters $(\dot{\gamma}_0, F_0, \widehat{\tau}_0, p, q)$, which have been determined for pure Al, see [44]. The uncoupled (i.e. the last term due to static recovery is not considered) hardening-recovery laws defined by Equations (77) and (78) contain six parameters $(C_\perp, C_\odot, K_\perp, K_\odot, d_\perp, d_\odot)$ which have been identified by [35] from experimental data previously obtained by [45]. The flow rule parameters are listed in Table 2 and those from the evolution equations in Table 3. Finally, the static recovery parameter C_{st} was chosen to be $10\,\mathrm{m\,J^{-1}}$, a value sufficiently large to annihilate most of the dislocations at the wake of a moving grain boundary.

In order to verify the validity of the numerical implementation and the parameters used, finite-element calculations of single crystals subject to uniaxial tensile loading were performed using the commercial code Zebulon [46]. The 3D mesh consisted of $44 \times 4 \times 4$ quadratic 3D elements with reduced integration (C3D2r). Nodes on each side of the opposite top and bottom faces were constrained from moving laterally to reproduce the grip constraints. As measured in [45], an initial misalignment of 0.5° in the Al single crystals away from the [100], [111] and [112] crystallographic orientations was introduced in the simulations carried out. A true strain rate of $7.5 \times 10^{-5}\,\mathrm{s^{-1}}$ was applied at a temperature of 273 K. A comparison between the predicted finite element stress–strain curves and the experimental data are shown in Figure 8, revealing good agreement.

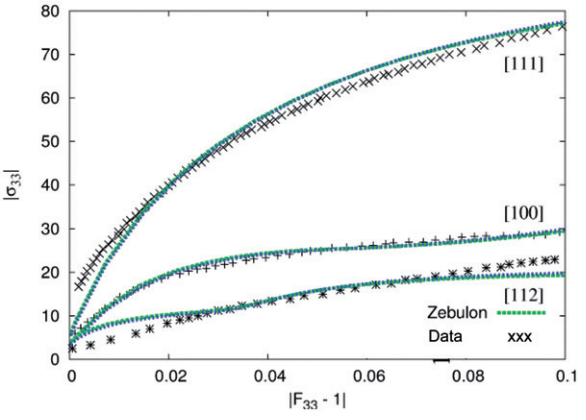

Figure 8. Comparison between the predicted true stress–strain response of Al along the [100], [111] and [112] crystal orientations with experiment data from [45] at 273 K.

5. Conclusions

In this work, we have introduced a novel a coupled phase field–crystal plasticity framework that accounts for the microstructural evolution driven by grain boundary curvature and/or stored energy. The coupled theory relies on two phase field variables to represent the continuous microstructure evolution through the grain boundary/interface regions. Its implementation in the finite element method relies on generalised stresses and their balance forces formulated within the framework of the thermodynamics of irreversible processes. The phase field model was formulated in 2D to enable the coupled formulation to be expressed using a simpler theoretical framework than in 3D. In particular, in-plane slip must be considered so that only in-plane lattice rotations develop, as required by the 2D phase field formulation. Future work will address 3D effects. Some of the most original aspects of this work are (i) the fact that the stored energy, and hence the dislocation densities generated during deformation, is incorporated explicitly in the free energy function of the phase field theory; and (ii) the static recovery-type mechanism which accounts for the annihilation of dislocations in the wake of migrating grain boundaries, and the finite element formulation and implementation of the couple formulations, a task not to be underestimated.

In this paper, the calibration of the main parameters of the coupled stress-phase field theory has been presented. In a companion paper [30], the theory will be validated against known data and analytical solutions, and the results of the evolution of polycrystalline aggregates during recrystalisation will be presented and discussed. It is hoped that the simulation and predictive capabilities of the coupled framework will provide an important theoretical framework for analysing micro-structural evolution phenomena required for the understanding and optimisation of thermo-mechanical processes. Although this study has been motivated by the application of recrystalisation processes, the coupled theory itself is not limited to such an application, and should be applicable to a wide variety of other situations

involving the interacting effects between plasticity and moving grain boundaries/interfaces.

Acknowledgements

This research was supported by the European Commission, project DIGIMAT (contract number NMP3-CT-2006-017105). This support is gratefully acknowledged.

References

[1] A. Khachaturyan, *The Theory of Structural Transformations in Solids*, Wiley & Sons, New York, 1983.
[2] Q. Bronchart, Y. Le Bouar and A. Finel, Phys. Rev. Lett. 100 (2008) p.157.
[3] A. Gaubert, Y. Le Bouar and A. Finel, Phil. Mag. 90 (2010) p.375.
[4] K. Ammar, B. Appolaire, G. Cailletaud, F. Feyel and S. Forest, Comput. Mater. Sci. 45 (2009) p.800.
[5] K. Ammar, B. Appolaire, G. Cailletaud and S. Forest, Eur. J. Comput. Mech. 18 (2009) p.485.
[6] K. Ammar, B. Appolaire, G. Cailletaud and S. Forest, Phil. Mag. Lett. 91 (2011) p.164.
[7] E.P. Busso, Int. J. Plast. 14 (1998) p.355.
[8] Y. Suwa, Y. Saito and H. Onodera, Mater. Sci. Eng. A 457 (2007) p.132.
[9] T. Takaki and Y. Tomita, Int. J. Mech. Sci. 52 (2010) p.320.
[10] D. Srolovitz, J. Vac. Sci. Tech. A 4 (1986) p.2925.
[11] P. Tavernier and J. Szpunar, Acta Metall. Mater. 39 (1991) p.557.
[12] A. Rollett, M. Luton and D. Srolovitz, Acta Metall. Mater. 40 (1992) p.43.
[13] V. Marx, F. Reher and G. Gottstein, Acta Mater. 47 (1999) p.1219.
[14] G. Gottstein, D. Molodov, L. Shvindlerman, D. Srolovitz and M. Winning, Curr. Opin. Solid State 5 (2001) p.9.
[15] J. Geiger, A. Roosz and P. Barkoczy, Acta Mater. 49 (2001) p.623.
[16] A. Soares, A. Ferro and M. Fortes, Scripta Metall. 19 (1985) p.1491.
[17] S. Gill and A. Cocks, Acta Mater. 44 (1996) p.4777.
[18] S. Osher and J. Sethian, J. Comput. Phy. 79 (1988) p.12.
[19] B. Serre, *Simulation Numérique 3d De La Croissance De Grains Par La Méthode Des Éléments Finis*, Ecole des Mines de Saint Etienne, France, 2007.
[20] I. Steinbach, F. Pezzolla, B. Nestler, M. Seesselberg, R. Prieler, G. Schmitz and J. Rezende, Physica D 94 (1996) p.135.
[21] L. Chen and D. Fan, J. Am. Ceram. Soc. 79 (1996) p.1163.
[22] N. Moelans, B. Blanpain and P. Wollants, Acta Mater. 54 (2006) p.1175.
[23] R. Kobayashi, J. Warren and W. Carter, Physica D 140 (2000) p.141.
[24] J. Warren, R. Kobayashi, A. Lobkovsky and W. Craig Carter, Acta Mater. 51 (2003) p.6035.
[25] M. Lusk, Proc. R. Soc. London, Ser. A 455 (1999) p.677.
[26] M. Gurtin and M. Lusk, Physica D 130 (1999) p.133.
[27] R. Vandermeer and B. Rath, Metall. Mater. Trans. A 20 (1989) p.1933.
[28] T. Takaki, A. Yamanaka, Y. Higa and Y. Tomita, J. Comput-Aided Mater. Des. 14 (2007) p.75.
[29] K. Cheong and E.P. Busso, Acta Mater. 52 (2004) p.5665.
[30] G. Abrivard, E.P. Busso, S. Forest and B. Appolaire, Phil. Mag. (2012) This issue.
[31] A. Lobkovsky and J. Warren, Phys. Rev. E 63 (2001) p.051606-1.

[32] E. Fried and M. Gurtin, Physica D 91 (1996) p.143.
[33] J. Bailey and P. Hirsch, Proc. R. Soc. London 267 (1962) p.11.
[34] J. Besson, G. Cailletaud, J.L. Chaboche, S. Forest and M. Blétry, *Non-linear Mechanics of Materials, Series: Solid Mechanics and Its Applications*, Vol. 167, Springer, Berlin, 2009. ISBN: 978-90-481-3355-0, 433p.
[35] K. Cheong, E.P. Busso and A. Arsenlis, Int. J. Plast. 21 (2005) p.1797.
[36] K. Cheong and E.P. Busso, J. Mech. Phys. Solids 54 (2006) p.671.
[37] E. Pouillier, A. Gourgues, D. Tanguy and E.P. Busso, Int. J. Plast. 34 (2012) p.139.
[38] E.P. Busso and G. Cailletaud, Int. J. Plast. 21 (2005) p.2212.
[39] G. Abrivard, *A Coupled Crystal Plasticity – Phase Field Formulation to Describe Microstructural Evolution in Polycrystalline Aggregates During Recrystalisation*, Ecole des Mines de Paris, France, 2009.
[40] W. Shockley and W. Read, Phys. Rev. 75 (1949) p.692.
[41] C. Yang, A. Rollett and W. Mullins, Scripta Mater. 44 (2001) p.2735.
[42] G. Gottstein, D. Molodov, L. Shvindlerman, D. Srolovitz and M. Winning, Curr. Opin. Solid State Mater. Sci. 5 (2001) p.9.
[43] G. Simmons and H. Wang, *Single Crystal Elastic Constants and Calculated Aggregates Properties*, The MIT Press, Cambridge, 1971.
[44] S. Balasubramanian and L. Anand, J. Mech. Phys. Solids 50 (2002) p.101.
[45] W. Hosford, R. Fleischer and W. Backofen, Acta Metall. 8 (1971) p.187.
[46] J. Besson, R. Le Riche, R. Foerch and G. Cailletaud, Revue Européenne des Éléments Finis 7 (1998) p.567.